Non-equilibrium adiabatic molecular dynamics simulations of methane clathrate hydrate decomposition

Alavi, Saman; Ripmeester, J.A.

Publisher's version / Version de l'éditeur:
https://doi.org/10.1063/1.3382341
The Journal of Chemical Physics, 132, 14, pp. 144703-1-144703-8, 2010-04-13

Nonequilibrium adiabatic molecular dynamics simulations of methane clathrate hydrate decomposition

Saman Alavi[1,2,a)] and J. A. Ripmeester[2,b)]
[1]*Department of Chemistry, University of Ottawa, Ottawa, Ontario K1N 6N5, Canada*
[2]*Steacie Institute for Molecular Sciences, National Research Council of Canada, Ottawa, Ontario K1A 0R6, Canada*

(Received 26 October 2009; accepted 16 March 2010; published online 13 April 2010)

Nonequilibrium, constant energy, constant volume (*NVE*) molecular dynamics simulations are used to study the decomposition of methane clathrate hydrate in contact with water. Under adiabatic conditions, the rate of methane clathrate decomposition is affected by heat and mass transfer arising from the breakup of the clathrate hydrate framework and release of the methane gas at the solid-liquid interface and diffusion of methane through water. We observe that temperature gradients are established between the clathrate and solution phases as a result of the endothermic clathrate decomposition process and this factor must be considered when modeling the decomposition process. Additionally we observe that clathrate decomposition does not occur gradually with breakup of individual cages, but rather in a concerted fashion with rows of structure I cages parallel to the interface decomposing simultaneously. Due to the concerted breakup of layers of the hydrate, large amounts of methane gas are released near the surface which can form bubbles that will greatly affect the rate of mass transfer near the surface of the clathrate phase. The effects of these phenomena on the rate of methane hydrate decomposition are determined and implications on hydrate dissociation in natural methane hydrate reservoirs are discussed. © *2010 American Institute of Physics*. [doi:10.1063/1.3382341]

I. INTRODUCTION

Large reservoirs of methane hydrate are found on continental margins in sediments under the ocean floor and under the permafrost in the Arctic.[1,2] The decomposition of these hydrate formations to produce natural gas, if done controllably, can lead to a huge source of relatively clean burning methane fuel.[3,4] However, uncontrolled hydrate decomposition has the potential to lead to a catastrophic release of methane (a potent greenhouse gas) into the atmosphere. It is therefore important to understand the details of the mechanism of the decomposition of methane in the presence of surface water layers under conditions mimicking methane hydrate reservoirs.

The decomposition of methane structure I (sI) clathrate hydrate has been extensively studied experimentally, with thermodynamic modeling and molecular simulations. Calorimetric measurements give a heat of dissociation of methane hydrate of 18.13 ± 0.27 kJ/mol (hydrate $\rightarrow$ ice + gas) at 273 K and 101 kP (Ref. 5) and 54.4 ± 1.4 kJ/mol of gas (hydrate $\rightarrow$ liquid + gas) at 292 K over a range of pressures up to 20 MPa.[6]

Macroscopic models of hydrate decomposition in reservoirs[3,4] often start with an assumption of intrinsic reaction kinetics. The intrinsic reaction kinetics mechanism[7–10] for methane hydrate decomposition assumes that, at constant temperature, the hydrate decomposition rate, $-dn_H/dt$, is proportional to the gradient in methane gas fugacity (concentration or pressure) between the solid methane hydrate phase, f_{hydrate}, and the nonequilibrium water-methane mixture at the interface, $f_{\text{interface}}$,

$$\frac{-dn_H}{dt} = k_d A_{HS}(f_{\text{interface}} - f_{\text{hydrate}}), \tag{1}$$

where k_d is the rate constant for the hydrate decomposition, and A_{HS} is the hydrate surface area per unit hydrate volume. The rate constant has been further analyzed in terms of the geometry of the solid clathrate phase surface (spherical nanoparticles or flat clathrate hydrate surface), the overtemperature (temperature above the stability of the clathrate hydrate phase), and thermal properties of the clathrate phase.[11] The rate constant is assumed to have Arrhenius-type temperature dependence with activation energy of E_{act} which must be provided before methane gas can be released from the hydrate,

$$k_d = k_d^0 \exp(-E_{\text{act}}/RT). \tag{2}$$

The intrinsic kinetics mechanism is used to explain measurements of methane hydrate decomposition in isothermal stirred-tank reactors where pressure and temperature gradients between the clathrate and water phases are eliminated as much as possible. Activation energies for the decompositions, E_{act}, determined from intrinsic kinetics are determined to be significantly higher (78 kJ/mol CH_4) than the heat of decomposition of the clathrate. Inherent in Eq. (1) is the assumption that hydrate decomposition occurs under isothermal conditions.

a)Electronic mail: saman.alavi@nrc-cnrc.gc.ca.
b)Electronic mail: john.ripmeester@nrc-cnrc.gc.ca.

Sloan and co-workers[12] studied the rate of methane hydrate decomposition in the presence of temperature differences between the water and solid hydrate phases. They assume that heat transfer from the liquid (at an initial temperature of T_i) to the clathrate phase occurs at the constant rate q_s. The liquid-solid hydrate interface then reaches a temperature T_s which is the equilibrium temperature for the three phase hydrate-water-methane gas system at the pressure of the experiment. This model assumes ablation of the water formed by hydrate decomposition by the released methane gas. The heat transfer mechanism has been combined with the intrinsic reaction kinetics mechanism by Jamaluddin and Bishnoi.[10]

Although the approximations of the intrinsic reaction kinetics and the heat transfer mechanism for hydrate decomposition seem reasonable, it is difficult to judge whether the commonly used assumptions inherent in these models correspond to the actual conditions of hydrate decomposition. In reality, the solution and solid hydrate phases can have considerably different temperatures with considerable temperature gradients near the interface. Additionally, in many cases, the solution phase is of finite size and cannot deliver heat at a constant rate to the solid hydrate interface. This will be particularly true in hydrate reservoirs where hydrate decomposition may be caused by a pressure drop. The assumption of the ablation of the "cold" water from the decomposing hydrate phase also needs to be verified under these conditions.

The decomposition of hydrate to water+methane gas is a phase change and should be treated analogous to the melting of ice placed in water. The melting of ice (for example, an ice cube) placed in water occurs via a gradual heat transfer from the liquid at temperature T_i, to the ice sample at a fixed temperature T_s=273 K (assuming ambient pressure). During the finite life time of the ice sample, the temperature of the solid portion remains constant at the melting point T_s while heat transfer from the liquid gradually melts more and more ice from the surface of the solid. The heat transfer rate depends on the temperature difference $T_i - T_s$ and shape of the ice sample. If the system is not stirred, a temperature gradient will be established between the liquid adjacent to the ice sample and the bulk liquid and which will contribute to the rate of heat transfer to the ice cube. Such a liquid state temperature gradient is expected to exist even in stirred systems due to no-slip boundary conditions at the ice surface. These factors will complicate the modeling of the ice sample melting.

Laidler has done a thorough analysis of the temperature dependence of rate constants.[13] He shows that over small temperature ranges it becomes possible to model the temperature dependence of a rate constant k, as $\ln k$ as a function of $1/T$, T, and $\ln T$. In homogenous gas phase reactions, the linear dependence of $\ln k$ on $1/T$ (Arrhenius plot) is taken as proof of the existence of an activation energy. However, for solid state processes occurring over a limited temperature range, the linear behavior of $\ln k$ versus $1/T$ is not sufficient proof of the presence of an activated chemical process. Using the analysis of Laidler, Galwey *et al.*[14] studied the rate of ice melting to determine whether melting can be modeled as a solid-state reaction (analogous to a homogenous phase reaction) with a rate constant that has a temperature dependence described by the Arrhenius equation and activation energy E_{act}. They observed that at temperatures relatively far from the melting point of ice (in the range of 304–278 K), the temperature dependence of the rate constant of melting can be superficially modeled with the Arrhenius equation. However, at temperatures close to the melting point (below 278 K), large negative deviations of the rate constant from the predicted Arrhenius behavior are seen. This is expected, since, at the melting point, the rate of melting should drop to zero, however, the Arrhenius equation does not predict this behavior. They conclude that melting must be modeled based on heat transfer between the warmer liquid water and solid ice which is always maintained at 273.15 K, and not as a solid-state reaction with homogenous temperature and "activation energy."

Galwey's analysis raises the question of whether similar Arrhenius behavior and activation energy-based models for the dissociation of methane hydrate are also only superficially correct for a limited temperature range far from the hydrate decomposition point and, in actuality, the rate of clathrate decomposition is controlled by heat transfer between the solid phase and the water solution. Analogous to the case of ice in water, the maximum temperature of a sample of solid methane hydrate in contact with the water phase is the equilibrium triple point of the system at the pressure of the simulation. It may not be physically reasonable to assume the solid methane hydrate phase can have an overtemperature higher than this value. Here, we present a preliminary examination of these issues.

Methane clathrate hydrate decomposition has been modeled extensively with molecular dynamics simulations. To date, most molecular dynamics simulations of the decomposition of methane hydrate nanospheres or bulk surfaces in contact with aqueous phases have been performed with constant temperature (thermostated) molecular dynamics simulations.[11,15–21] In all cases the hydrate decomposition is driven by the overtemperature of the hydrate-liquid system compared to the equilibrium temperature of these two phases. Báez and Clancy[15] observed a stochastic and stepwise decomposition of the hydrate nanospheres where portions of the hydrate surface decompose simultaneously. English *et al.*[20] verified this observation and additionally concluded that diffusion of methane through the surface liquid layer in the hydrate strongly affects the decomposition rate. Myshakin *et al.*[21] used overtemperatures of up to 30 K above the clathrate decomposition point and observed Arrhenius behavior for the temperature behavior of the methane hydrate decomposition rate. Finally, English and Phelan[11] simulated the decomposition of methane hydrate nanospheres and bulk surfaces with different overtemperatures considering both mass transfer and overtemperature terms in calculating the rate of decomposition. Vatamanu and Kusalik[22] modeled the process of methane hydrate formation from the liquid phase, but they use localized heat sources and enhanced methane delivery rates to the hydrate surface to accelerate the hydrate formation process. These will affect the rate of hydrate phase formation.

Previous simulations were performed with thermostats under isothermal conditions, i.e., molecular velocities of molecules in the hydrate and solution phases are rescaled to maintain a target simulation temperature. In such simulations, temperature gradients will not be established between the solid hydrate and the neighboring solution phase during clathrate decomposition. Thermal gradients can have an important effect on slowing the rate of further decomposition of the clathrate phase. If such a thermal gradient is established in the real system, heat transfer from the bulk liquid to the clathrate surface will be required before further clathrate decomposition can occur. A rigorously stirred system may remove some effects of the thermal gradient, but due to the molecular-scale nature of the thermal gradient and no-slip boundary conditions, the temperature gradient will not be totally eliminated.

The thermal gradients between the hydrate surface and bulk solution may also impede the diffusion of methane released from the hydrate surface to the bulk liquid (and presumably into the gas phase). Methane confined near the hydrate surface may promote the reformation of clathrate hydrate cages. A rigorously stirred system may remove some mass transfer effects, but due to the molecular scale of the phenomenon and no-slip boundary conditions, it is likely that methane concentration gradients will not be totally eliminated. English and Phelan recognize these limitations of isothermal simulations in realistically describing the clathrate decomposition process.[11]

It is for the above reasons that in the present simulations we have performed constant volume-constant energy (*NVE*) molecular dynamics simulations to explicitly observe the nature of the heat and mass transfer during clathrate hydrate decomposition. We believe *NpT* or *NVT* simulations which "equilibrate" the temperature between the hydrate phase and the aqueous phase do not reflect the nature of the hydrate decomposition process. The goal is to gain a better phenomenological and semiquantitative understanding of the hydrate decomposition process. The details of the molecular dynamics simulations used in this study are described in Sec. II. Results and discussion follow in Sec. III and the paper ends with a summary and conclusions in Sec. IV.

II. MOLECULAR DYNAMICS METHODS

The initial input structures for the clathrate oxygen atoms correspond to those in the experimental sI clathrate hydrate[23] with the positions of the configurationally disordered water hydrogen atoms chosen by a Monte Carlo procedure which minimizes the dipole moment of the unit cell[24] in a manner consistent with the Bernal–Fowler ice rules.[25]

The extended simple point charge (SPC/E) model[26] is used for water. The CH_4 molecules are considered to be rigid, with a C–H bond length of 1.0895 Å which corresponds to the experimental gas-phase value. The Lennard-Jones parameters and electrostatic point charges for the carbon and hydrogen atoms of methane were chosen from the Murad and Gubbins potential.[27] The intermolecular potential is given as

TABLE I. Atomic partial charges and Lennard-Jones interaction parameters for SPC/E water and the rigid CH_4 molecules used in the MD simulations.

Atom	q (e)	σ_{ii} (Å)	ε_{ii} (kJ/mol)
O (water)	−0.8476	3.166	0.6502
H (water)	+0.4238	0.000	0.0000
C (methane guest)	−0.56	3.64	1.365
H (methane guest)	+0.14	0	0

$$V(r_i,r_j)=\sum_{i,j}4\varepsilon_{ij}\left[\left(\frac{\sigma_{ij}}{r_{ij}}\right)^{12}-\left(\frac{\sigma_{ij}}{r_{ij}}\right)^{6}\right]+\frac{1}{4\pi\varepsilon_0}\frac{q_iq_j}{r_{ij}}, \quad (3)$$

where each summation indices runs over atom sites in different molecules. The values of the parameters used for the intermolecular potentials are given in Table I. Standard combination rules, $\varepsilon_{ij}=\sqrt{\varepsilon_{ii}\varepsilon_{jj}}$ and $\sigma_{ij}=(\sigma_{ii}+\sigma_{jj})/2$, are used for the Lennard-Jones potential parameters between unlike force centers in water and CH_4. Mastny and de Pablo[28] and English and Phelan[11] used the combination of TIP4P for water-water interactions, the OPLS-all atom potential for methane-methane interactions, and the Sun and Duan potential from *ab initio* calculations[29] for water-methane interactions, to accurately model the melting point of methane hydrate. For the purposes of our study, the intermolecular potential used should be of sufficient accuracy (see below).

Simulations were performed with the DL_POLY program version 2.17.[30] The equations of motion were integrated with a time step of 1 fs. Coulombic long-range interactions were calculated using Ewald summation methods[31] with a 1×10^{-6} precision and all interatomic interactions in the simulation box were calculated within a cutoff distance of $R_{\text{cutoff}}=15.0$ Å.

To test the force field for methane in water, we calculated the diffusion coefficient for methane in water. Simulations of ten methane molecules in 1242 water molecules were performed for seven temperatures in the range of 273–310 K. The solutions were first equilibrated with a *NpT* simulation for 100 ps (with 50 ps equilibration) and the resulting configuration was simulated for 200 ps (with 50 ps equilibration) in a *NVE* simulation. In the *NpT* simulations, the Nosé–Hoover thermostat-barostat algorithms[32] were used with 0.5 and 2.0 fs relaxation times, respectively. The temperature dependence of the methane diffusion coefficients in water are plotted as an Arrhenius plot in Fig. 1. The activation energy for the diffusion of methane is 29 ± 3 kJ/mol which agrees reasonably well with the 24.7 kJ/mol activation energy determined experimentally.[33,34]

The clathrate-water system was equilibrated in two stages. First a $3\times3\times6$ replica of the sI methane clathrate hydrate unit cell with full methane occupancy in small and large unit cells was prepared. Equilibrated samples of water at each temperature with the same xy cross section as the clathrate phase and a total of 1800 water molecules were placed above and below the clathrate (along the z-direction) phase for a total of 20 412 atoms in the simulation. These water phases are allowed to equilibrate over the frozen hydrate phase surface in *NVT* molecular dynamics simulations

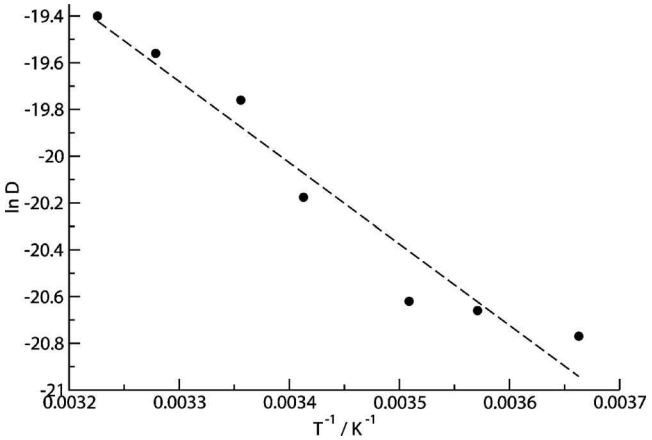

FIG. 1. The temperature dependence of the methane diffusion coefficient in water at temperatures between 273 and 310 K from simulations with the SPC/E potential for water and the Murrad–Gubbins potential for methane. Arrhenius-like behavior is obtained for the diffusion with an activation energy of 26 kJ/mol.

for 200 ps. These simulations were followed by a further 200 ps of *NpT* simulations at a pressure of 0.1 kbar (with frozen clathrate phase) to allow the water to equilibrate on the clathrate surface at the target temperature and pressure. The energies and other thermodynamic variables for water in contact with the clathrate hydrate phase were sufficiently converged within these overall simulation times. Snapshots of a typical methane clathrate hydrate-water surface configuration after the setup stages is shown in Fig. 2. Four temperatures for hydrate dissociation were considered, namely, 273, 290, 300, and 310 K.

Once the water in the two-phase system was equilibrated, a new *NVE* adiabatic simulation was begun with the molecules of the methane hydrate unfrozen. To impart kinetic energy to the molecules of the clathrate hydrate phase, the water and hydrate phases were equilibrated for a short time of 5 ps. The *NVE* clathrate hydrate+liquid water simulations were then initiated and run for 450 ps and the clathrate decomposition monitored throughout these final simulations. A typical methane clathrate hydrate-water interface after the beginning of the simulation is shown in Fig. 3. An alternative methodology would be to separately thermostat the water and hydrate phases to different temperatures. We will pursue these simulations in future work.

III. RESULTS AND DISCUSSION

Sample snapshots for the simulation with an initial temperature of 310 K for times up to 400 ps after the beginning of the simulation are shown in Fig. 4. From these snapshots (and from animations of the simulation), the decomposition of rows of methane hydrate are seen to occur concertedly, an observation made in previous simulation studies.[15,11] Individual methane molecules from small and large cages are occasionally released from the clathrate phase into the water, but if the neighboring clathrate framework is intact, these molecules are often reincorporated into a reconstructed clathrate hydrate cage. Only when an entire row of clathrate hydrate cages (roughly a row of unit cells) decomposes does the clathrate decomposition become irreversible. The fact

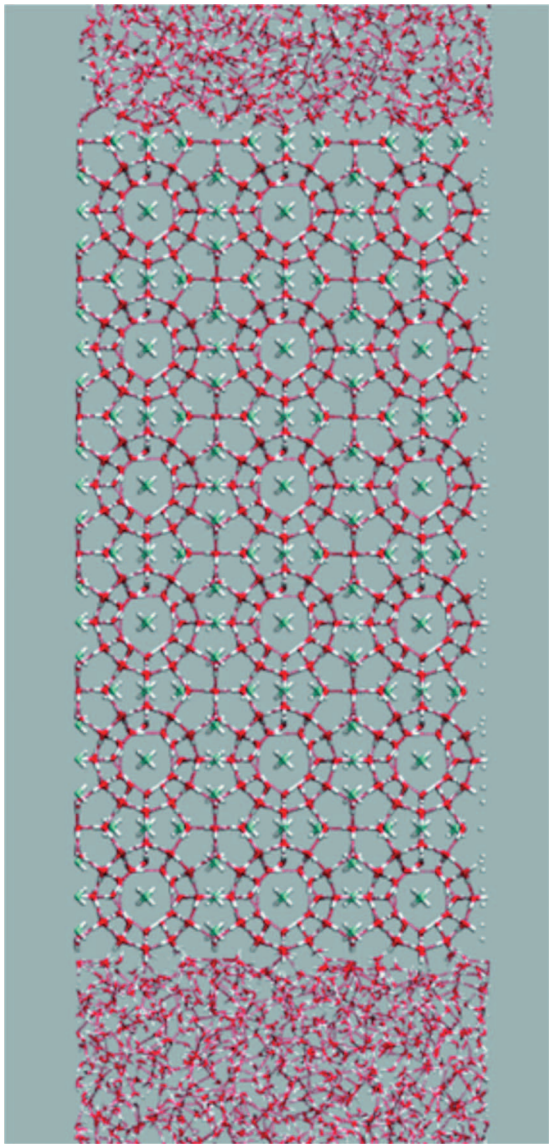

FIG. 2. A snapshot of the interface between a sI clathrate hydrate surface and water at the beginning of a simulation at 290 K and 0.1 kbar. The clathrate phase is frozen and water allowed to equilibrate on the clathrate hydrate surface.

that rows of clathrate hydrate cages decompose simultaneously to release the methane gas may explain why the observed "activation energy" of the clathrate dissociation in the intrinsic kinetics mechanism appears so large (78 kJ/mol) compared to the hydrate enthalpy of dissociation (54 kJ/mol).

An additional complication to the simple modeling of the clathrate hydrate decomposition is seen in Fig. 4 for times after 200 ps. During dissociation, large amounts of methane gas are released from the clathrate hydrate and "bubbles" form near the hydrate-solution interface. These bubbles will affect heat and mass transfer at the clathrate surface. Methane bubble formation has been observed during the dissociation of methane hydrate crystals in a glass micromodel used to mimic the conditions of methane hydrate dissociation in sediments.[35]

The snapshots of the simulations after 400 ps for systems with initial temperatures in the range of 273–310 K are

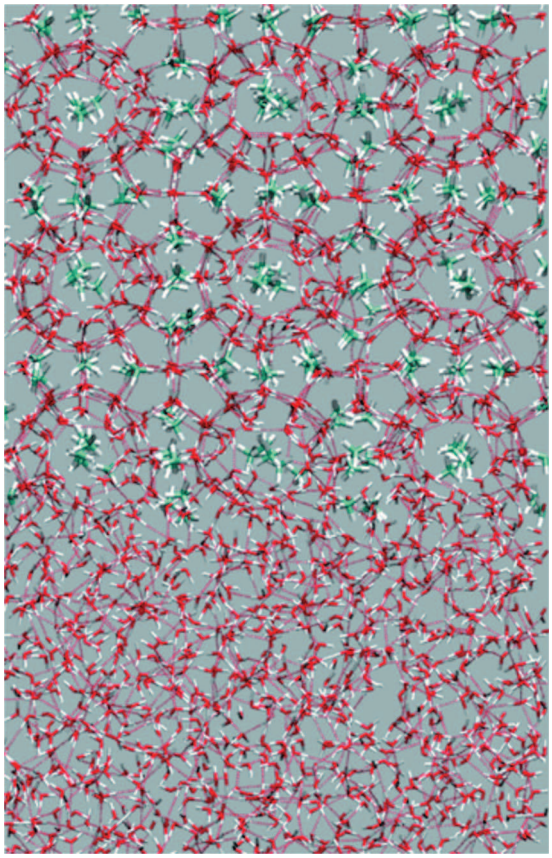

FIG. 3. A snapshot of the interface between the sI clathrate hydrate surface and water after removing restraints on the clathrate hydrate motion. Dashed lines indicate hydrogen bonding.

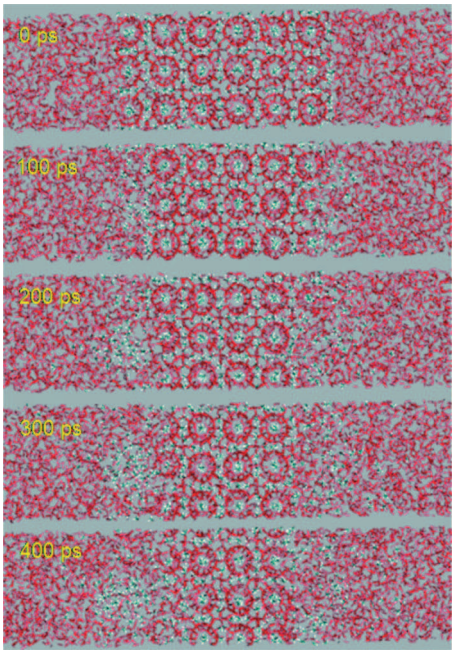

FIG. 4. Snapshots of the simulation with an initial temperature of 310 K after 100 to 400 ps. The formation of a methane gas bubble (left hand solution phase) can lead to strong mass and heat transfer effects between the bulk water and clathrate surface.

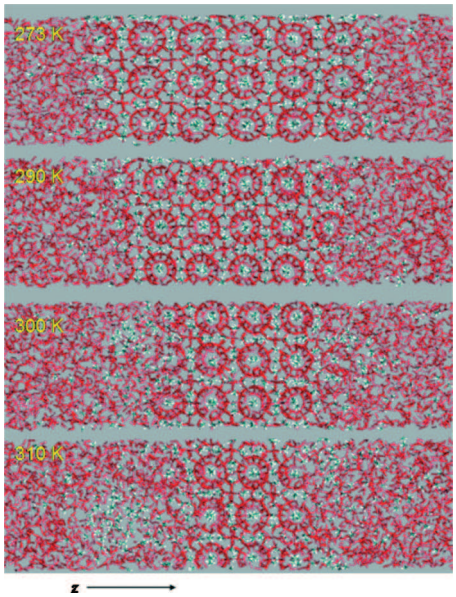

FIG. 5. Snapshots of final configurations of simulations with initial temperatures in the range of 273–310 K. As expected, the amount of decomposition of the clathrate correlates with the initial temperature of the simulation cell.

shown in Fig. 5. The hydrate phase is seen to be stable at 273 K. There is a small release of methane into the aqueous phase at this temperature which is due to the incomplete nature of the sI clathrate hydrate cages at the interface with the water phase. However, we do not observe the formation of the methane bubble in the simulation at 273 K. This shows that the methane bubble observed at higher temperatures (300 and 310 K) is due to the release of methane from additional hydrate decomposition and not release from the initial surface cages. Considerable clathrate hydrate decomposition occurs for temperatures greater than 300 K.

Plots of the average simulation temperature and pressure for the entire systems as a function of the simulation time for the *NVE* (adiabatic) simulations are shown in Fig. 6. At the initial higher temperatures where considerable clathrate hydrate decomposition occurs, there is a large temperature drop (>10 °C) during the simulation as the hydrate decomposes and kinetic energy is consumed.

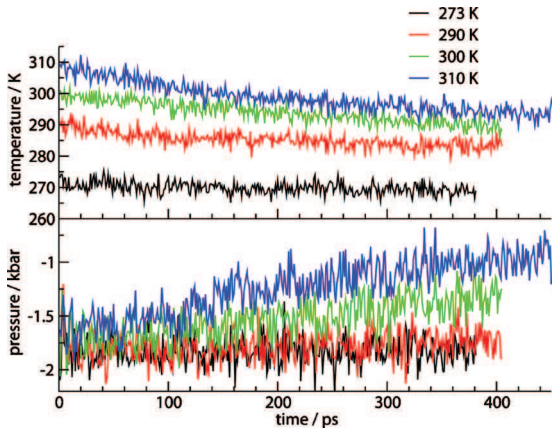

FIG. 6. The time dependence of the average system temperature (top panel) and pressure (bottom panel) from the clathrate-water *NVE* simulation with initial temperatures in the range of 273–310 K. The increase in pressure with time for the high temperature runs is related to the release of methane gas into the system from the hydrate phase as the hydrate decomposes.

The total pressure in the system increases for temperatures where considerable hydrate dissociation occurred. Under constant volume conditions, the pressure rise that results from the release of methane gas in the system may drive the system into the hydrate stability zone of the phase diagram and lead to self-stabilization and a stoppage in the hydrate dissociation process. From the last frame of Fig. 4, this does not seem to have occurred, even at the highest temperature of the simulations 310 K. The negative values obtained for the pressures of the *NVE* simulations merits some comment. It is well known that calculated lattice constant for clathrate hydrates for the SPC/E and other nonpolarizable water potentials underestimate the experimental lattice constants by 1%–5%.[36] In the present simulations, the initial configuration of the methane hydrate phase is obtained from the experimental x-ray structure. Since we have only given translational freedom to the clathrate hydrate phase in the *NVE* stage of the simulations, there is residual tension in the hydrate phase leading to the observed negative pressures in Fig. 6. The negative system pressure can affect quantitative aspects of methane gas release in the present simulations, but we believe qualitative aspects of the hydrate decomposition are captured correctly with the present setup. For example, the rate and size of methane bubble formation may be affected by the system pressure, but arguments regarding the importance of heat and mass transfer to the hydrate decomposition process are not affected.

In reality, hydrate dissociation occurs under constant pressure conditions and the release of methane gas may be faster than calculated here. However, we believe it is crucial not to impose the artificial thermostat constraints on the hydrate-liquid system and to maintain the nonequilibrium nature of the hydrate dissociation process in the simulation. For this reason, we perform *NVE* rather than *NpT* simulations which maintain constant system pressure.

In addition to an overall drop in system temperature, clathrate decomposition causes temperature gradients to be established between different parts of the clathrate/water system. Even if the clathrate+water system experimentally is in a stirred thermostated bath, there is finite time lag for the heat to diffuse from the bulk, through the no-slip boundary layer, to the clathrate surface. To study the magnitude of temperature gradients, the simulation cell was divided up into ten "slices" along the z-direction. For the system with an initial temperature of 310 K, the time variations of three of these slices during the simulation are shown in Fig. 7. The outer boundaries of each slice are indicated by arrows. Numbers of water and methane molecules in each slice are also shown as a function of time.

We observe that the temperatures of the three sample slices of the simulation cell are in the vicinity of 310 K at the beginning of the simulation. This is the result of the short 5 ps equilibration time allotted to the (clathrate hydrate +water) system prior to the beginning of the *NVE* simulation. The slice on the outermost part of the water phase (on the left) shows little change in average temperature or methane concentration. In the central slice which mostly encompasses the solid hydrate phase, there is a relatively small loss of methane molecules as a result of the decomposition of the

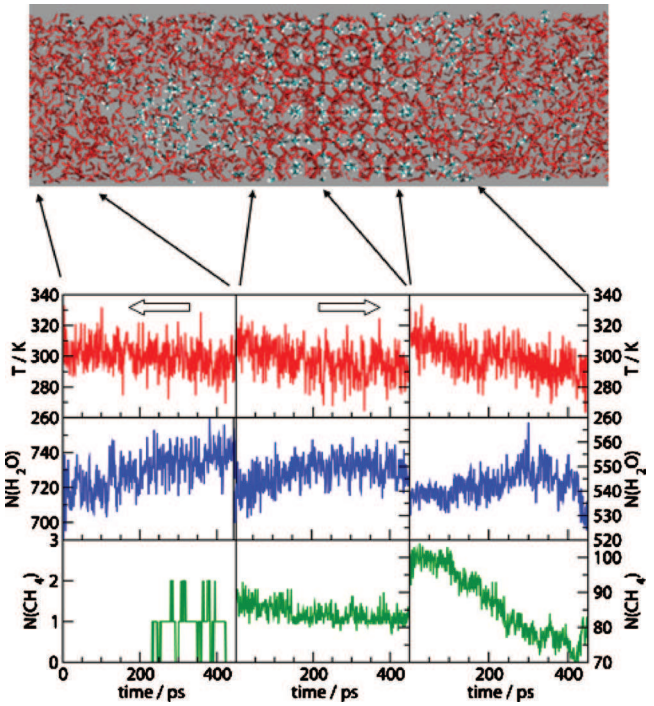

FIG. 7. The variation of the temperature, number of water molecules $N(H_2O)$, and number of methane molecules $N(CH_4)$ with time for three different slices in the z-direction of the sI methane hydrate simulation at 310 K. The final configuration of the simulation box is shown.

hydrate phase (on the left hand side of this slice) and diffusion of the methane into the solution. This layer shows a small temperature drop which occurs at the same time as the hydrate phase dissociates (as evidenced by the increase of the number of water molecules in the slice). In the right hand slice, more than half of the original hydrate phase has decomposed after 400 ps. There is a steady temperature drop as the methane hydrate melts and the methane molecules diffuse out of this region. In the slices where the clathrate phases decompose, temperature gradients as large as 20 K are established over time.

A number of different criteria have been used to specify the number of water[16,20] and methane[21] molecules in the solid hydrate or water phases in a methane hydrate decomposition simulation. These are based on the local structure of water molecules in the phase and the number water molecules coordinating a given methane molecule, respectively. In this work, the criterion for characterizing methane molecules as belonging to the hydrate phase or the solution phase is based on the Lindemann index.[37] At time $t=0$, all $8\times 54=432$ methane molecules are in the hydrate phase. At subsequent time steps, if a methane molecule has moved less than 8 Å (the approximate diameter of the sI clathrate large cages) with respect to its initial location, we consider the methane to be in the hydrate phase. Otherwise the cage holding this methane has decomposed and the methane molecule is removed from the hydrate count. In formulas, if for molecule i,

$$|\mathbf{r}_i(t)-\mathbf{r}_i(0)|<8\ \text{Å}\rightarrow i\in N(\text{hydrate};t). \tag{4}$$

We considered two variants to this condition. In the first case, if a methane molecule is removed from the hydrate

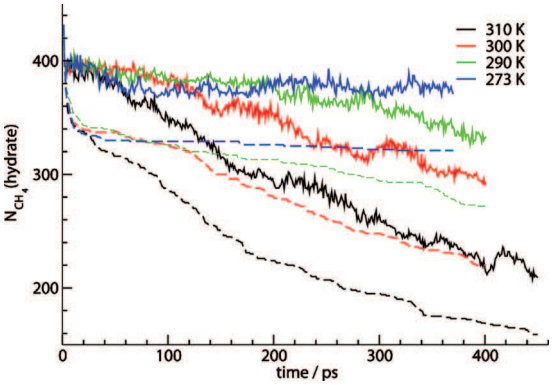

FIG. 8. The changes in the number of methane molecules in the hydrate phase as a function of simulation time for different starting temperatures. The dashed curves neglect cage reformation and recapture of the methane molecules from the solution phase. See text for further discussion.

phase at any prior time, it is excluded from methane count of the hydrate phase, $N(\text{hydrate};t)$ for all later times. In Fig. 8, we show the number of methane molecules in the solid hydrate phase as a function of time for systems with different initial temperatures. The dashed lines shown in Fig. 8 are based on this definition. This definition overestimates the rate of hydrate dissociation since it excludes the possibility of cage reformation and reincorporation of methane from the solution into the clathrate phase which is clearly seen in some animations of hydrate decomposition.

The second variant is to consider the condition given by Eq. (4) for each methane molecule, independent of the previous location of the methane molecules. This allows for the possibility of cage reformation, where a methane molecule returns to the cage site it started out in. This admittedly does not allow the possibility of methane molecules being incorporated into cage sites other than those they started out in, and so it can be considered as an upper limit to the rate of hydrate dissociation. This case is shown by the full lines of Fig. 8. In the second case, released methane molecules near the surface that get reincorporated into the hydrate phase are counted in the $N(\text{hydrate};t)$ class.

The decreases in $N(\text{hydrate};t)$ are parallel for both definitions (dashed and solid lines) and both give similar *rates* for the hydrate dissociation. The quick initial drop in the number of methane molecules in the hydrate phase in the first 20 ps of the simulation is related to the dissociation of the surface cages seen on the left hand side of the 0 ps simulation shown in Fig. 4. The methane bubble formation event at 310 K shown in Fig. 4 occurs 200 ps after the start of the simulation. This time is significantly later than the 20 ps time range of initial decomposition of the surface cages. The bubble formation therefore is not related to the initial release of methane molecules from the surface cages.

In Fig. 8 we see the rate of the hydrate dissociation decreases over time as the existing kinetic energy of the system is expended on clathrate heat of dissociation (see Fig. 5). This has important implications on modeling of hydrate dissociation in reservoirs. Another observation is the stepwise dissociation of the hydrate.

A row of hydrate unit cells in the simulation has $8\times3\times3=72$ methane molecules. This is consistent with the offset of the two sets of data in Fig. 8. The outermost layer of hydrate may participate in hydrate dissociation-reformation. The hydrate dissociation rates obtained from Fig. 8 could likely be fit to Arrhenius curve, but this would not necessarily be relevant to the dissociation mechanism as there is no real activation barrier to the hydrate dissociation, but rather mass and heat transfer barriers. Such an apparent "activation energy" would depend on the size of the system and the relative amounts of solid and liquid phases present. It is the interconversion of kinetic to potential energy, mass flow, and heat flow which drives the dissociation kinetics.

IV. SUMMARY AND CONCLUSIONS

We performed simulations of methane clathrate decomposition under adiabatic (*NVE* ensemble) conditions. We make several observations that are relevant to the proper modeling of the methane hydrate decomposition process in a reservoir:

(1) Decomposition does not occur in a homogenous manner (in time), but rather in a series of decomposition events where rows of clathrate cages decompose almost simultaneously.
(2) The simultaneous release of methane gas from rows of clathrate hydrate cages can lead to the formation of methane microbubbles near the clathrate surface. Methane molecules in these bubbles migrate away from the surface collectively in a heterogeneous manner which may not follow Fick's law.
(3) As the clathrate cages decompose, temperature gradients of up to 20 K can be established over time and across different segments of the clathrate and solution phase. These gradients can lead to substantial heat transfer effects.

Given the complex nature of the clathrate hydrate decomposition, the macroscopic modeling of the methane hydrate decomposition process under adiabatic conditions is difficult. A picture assuming isothermal hydrate and liquid phase conditions during the decomposition seems inconsistent with the nature of the first order phase transition of methane hydrate dissociation. Diffusion of released methane gas from the hydrate surface is not homogenous and the solution phase will not necessarily be isothermal over short time periods. Extracting an "activation energy" from the temperature dependence of the rate constant is also problematic because the hydrate dissociation rate constant captures many nonequilibrium effects during the decomposition process. Given these observations, we believe the time is apt for revisiting the modeling of reservoir methane hydrate decomposition processes within a new framework.

ACKNOWLEDGMENTS

The authors would like to thank an anonymous reviewer for the critical reading of the manuscript and helpful comments. We acknowledge Natural Resources Canada (NRCan) under the program "Gas Hydrates as a Canadian Energy Al-

ternative" for partial funding of this research. The support of the National Research Council of Canada is also gratefully acknowledged.

[1] G. J. MacDonald, Annu. Rev. Energy **15**, 53 (1990).
[2] A. V. Milkov, G. E. Claypool, Y.-J. Lee, W. Xu, G. R. Dickens, W. S. Borowski, and the Ocean Drilling Program Leg 204 Scientific Party, Geology **31**, 833 (2003).
[3] Y. Masuda, M. Kurihara, H. Ohuchi, and T. Sato, "A field scale simulation study on gas productivity of formations containing gas hydrates, Proceedings of the 4th Int'l Conf. Gas Hydrates, Yokohama, 2002, pp. 40–46.
[4] H. Hong and M. Pooladi-Darvish, J. Can. Pet. Technol. **44**, 39 (2005).
[5] Y. P. Handa, J. Chem. Thermodyn. **18**, 915 (1986).
[6] A. Gupta, J. Lachance, E. D. Sloan, Jr., and C. A. Koh, Chem. Eng. Sci. **63**, 5848 (2008).
[7] H. C. Kim, P. R. Bishnoi, R. A. Heidemann, and S. S. H. Rizvi, Chem. Eng. Sci. **42**, 1645 (1987).
[8] M. Clarke and P. R. Bishnoi, Chem. Eng. Sci. **55**, 4869 (2000).
[9] M. Clarke and P. R. Bishnoi, Ann. N.Y. Acad. Sci. **912**, 556 (2000).
[10] A. K. M. Jamaluddin, N. Kalogerakis, and P. R. Bishnoi, Can. J. Chem. Eng. **67**, 948 (1989).
[11] N. J. English and G. M. Phelan, J. Chem. Phys. **131**, 074704 (2009).
[12] J. W. Ullerich, M. S. Selim, and E. D. Sloan, AIChE J. **33**, 747 (1987).
[13] K. J. Laidler, J. Chem. Educ. **61**, 494 (1984).
[14] A. K. Galwey, D. B. Sheen, and J. N. Sherwood, Thermochim. Acta **375**, 161 (2001).
[15] L. A. Báez and P. Clancy, Ann. N.Y. Acad. Sci. **715**, 177 (1994).
[16] L. A. Báez, Ph.D. thesis, Cornell University, 1996.
[17] P. M. Rodger, Ann. N.Y. Acad. Sci. **912**, 474 (2000).
[18] K. Yasuoka and S. Murakoshi, Ann. N.Y. Acad. Sci. **912**, 678 (2000).
[19] N. J. English and J. M. D. MacElroy, J. Chem. Phys. **120**, 10247 (2004).
[20] N. J. English, J. K. Johnson, and C. E. Taylor, J. Chem. Phys. **123**, 244503 (2005).
[21] E. M. Myshakin, H. Jiang, R. P. Warzinski, and K. D. Jordan, J. Phys. Chem. A **113**, 1913 (2009).
[22] J. Vatamanu and P. G. Kusalik, J. Phys. Chem. B **110**, 15896 (2006).
[23] T. C. Mak and R. K. McMullan, J. Chem. Phys. **42**, 2732 (1965).
[24] E. P. van Klaveren, J. P. J. Michels, J. A. Schouten, D. D. Klug, and J. S. Tse, J. Chem. Phys. **114**, 5745 (2001); **115**, 10500 (2001); **117**, 6636 (2002).
[25] J. D. Bernal and R. H. Fowler, J. Chem. Phys. **1**, 515 (1933).
[26] H. J. C. Berendsen, J. R. Grigera, and T. P. Straatsma, J. Phys. Chem. **91**, 6269 (1987).
[27] S. Murad and K. E. Gubbins, in *Computer Modeling of Matter*, edited by P. Lykos (American Chemical Society, Washington, D.C., 1978), p. 62.
[28] E. A. Mastny and J. J. de Pablo, J. Chem. Phys. **129**, 034701 (2008).
[29] R. Sun and Z. H. Duan, Geochim. Cosmochim. Acta **69**, 4411 (2005).
[30] *DLPOLY 2.17*, edited by T. R. Forester and W. Smith (CCLRC, Daresbury Laboratory, Daresbury, 1995).
[31] D. Frenkel and B. Smit, *Understanding Molecular Simulation* (Academic, San Diego, 2000); M. P. Allen and D. J. Tildesley, *Computer Simulation of Liquids* (Oxford Science, Oxford, 1987).
[32] S. Nosé, J. Chem. Phys. **81**, 511 (1984); W. G. Hoover, Phys. Rev. A **31**, 1695 (1985); S. Melchionna, G. Ciccotti, and B. L. Holian, Mol. Phys. **78**, 533 (1993).
[33] P. A. Witherspoon and D. N. Saraf, J. Phys. Chem. **69**, 3752 (1965).
[34] D. Leek and J. A. Ripmeester (unpublished).
[35] D. Katsuki, R. Ohmura, T. Ebinuma, and H. Narita, J. Chem. Phys. **104**, 083514 (2008).
[36] C. Vega, E. Sanz, and J. L. F. Abascal, J. Chem. Phys. **122**, 114507 (2005); S. Alavi, J. A. Ripmeester, and D. D. Klug, *ibid.* **123**, 024507 (2005); S. Alavi, R. Susilo, and J. A. Ripmeester, *ibid.* **130**, 174501 (2009).
[37] F. A. Lindemann, Phys. Z. **11**, 609 (1910).